

Plane-Wave Theory of Self-Doubling Optical Parametric Oscillators

Orhan Aytür, *Member, IEEE*, and Yamaç Dikmelik, *Student Member, IEEE*

Abstract—This paper presents a theoretical analysis of self-doubling optical parametric oscillators (OPO's) where a single nonlinear crystal is used for both parametric generation and frequency doubling. In these devices, the parametric generation and frequency-doubling processes are both phase matched for the same direction of propagation inside the crystal. Different polarization geometries for which this simultaneous phase-matching condition can potentially be satisfied are identified and categorized. Plane-wave coupled-mode equations are presented for each of these categories. Numerical solutions of these coupled-mode equations and calculation of the single-pass saturated signal gain are outlined. Intracavity signal photon flux calculations based on these numerical solutions are presented. The dependence of performance measures such as the photon conversion efficiency on various design parameters are investigated.

Index Terms—Nonlinear frequency conversion, optical parametric oscillators, parametric devices, second-harmonic generation.

I. INTRODUCTION

OPTICAL parametric oscillators (OPO's) are widely used for tunable wavelength conversion of lasers to previously unavailable wavelength ranges [1]–[3]. By itself, an OPO can only provide downconversion to longer wavelengths. Upconversion to shorter wavelengths is achieved with the use of a second nonlinear element for frequency doubling [4] or sum-frequency generation [5]. This second nonlinear crystal is usually internal to the OPO cavity to take advantage of the high intracavity field intensities. The plane-wave theory of these two-crystal intracavity upconversion OPO's have been studied extensively [6]–[8]. Recently, a self-doubling OPO that employs a *single* nonlinear crystal for both parametric generation and frequency doubling has been reported [9]. This new device provides a highly efficient scheme for frequency upconversion of lasers. In this paper, we present a plane-wave theory of the self-doubling OPO.

II. SECOND-ORDER NONLINEAR INTERACTIONS

A second-order ($\chi^{(2)}$) nonlinearity results in the coupled interaction of three fields whose frequencies are related by $\omega_3 = \omega_1 + \omega_2$ [10]. For collinear monochromatic plane waves

$$E_m(z, t) = \text{Re}[E_m \exp(j(\omega_m t - k_m z))], \quad m = 1, 2, 3 \quad (1)$$

with complex field amplitudes E_m , the coupled-mode equations that describe this interaction (under the slowly varying envelope approximation) are [11]

$$\frac{dE_1}{dz} = -j \frac{\omega_1 d_e}{n_1 c} E_3 E_2^* e^{-j\Delta k z} \quad (2)$$

$$\frac{dE_2}{dz} = -j \frac{\omega_2 d_e}{n_2 c} E_3 E_1^* e^{-j\Delta k z} \quad (3)$$

$$\frac{dE_3}{dz} = -j \frac{\omega_3 d_e}{n_3 c} E_1 E_2 e^{+j\Delta k z} \quad (4)$$

where d_e is the effective nonlinear coefficient, n_m are the refractive indices, and $\Delta k = k_3 - k_1 - k_2$ is the wavevector mismatch. The initial conditions at the input facet of the nonlinear crystal determine whether the interaction results in second-harmonic, sum-frequency, difference-frequency, or parametric generation.

The phase (wavevector) mismatch Δk plays an important role in all of these interactions. When Δk is different from zero, momentum conservation is violated and the interactions become very weak [10]. The phase-matching condition, $\Delta k = 0$, has to be satisfied for efficient conversion of energy from one frequency to the other. Phase matching is mostly achieved by utilizing the natural birefringence of nonlinear crystals [12], [13].

A pump field at ω_3 and a signal field at ω_2 at the input result in an optical parametric amplifier (OPA), where the signal gets amplified and, in the process, an idler field at ω_1 is generated [11]. The parametric gain experienced by the signal field is subject to saturation as the pump and signal fields become comparable in intensity. A singly resonant OPO is constructed by placing the OPA inside a cavity that is resonant at the signal frequency. Oscillation starts if the unsaturated gain is higher than all cavity losses combined. The intracavity signal intensity assumes such a value that the saturated gain compensates for the cavity losses exactly. A partially reflecting mirror is usually employed for coupling the signal out of the cavity. The idler leaves the cavity through a dichroic beamsplitter that is highly transmitting at the idler frequency.

In an OPA, the lack of an idler field at the input of the crystal results in field solutions whose intensities are independent of the relative phase of the pump and the signal. This results in the well-known robust behavior of singly resonant OPO's, where the generated idler adjusts its phase to compensate for the phase fluctuations in the input pump and signal beams. Utilizing this freedom in the choice of initial phases, it is possible to convert the three coupled-mode equations for the complex field amplitudes to three real equations.

Manuscript submitted April 21, 1997; revised September 3, 1997. This work was supported in part by the Turkish Scientific and Technical Research Council (Tubitak) under Grant EEEAG-118.

The authors are with the Department of Electrical and Electronics Engineering, Bilkent University, TR-06533 Bilkent, Ankara, Turkey.

Publisher Item Identifier S 0018-9197(98)01776-X.

It is convenient to define normalized and real field amplitudes a_m such that $\phi_m = a_m^2$ represent the photon flux densities at each frequency ω_m . In doing this, we choose the phases of E_m such that the required phase relation for the OPA is satisfied and define the real and normalized amplitudes a_m through

$$E_1 = -j\sqrt{2\hbar\omega_1/n_1c\epsilon_0} a_1$$

$$E_2 = \sqrt{2\hbar\omega_2/n_2c\epsilon_0} a_2$$

and

$$E_3 = \sqrt{2\hbar\omega_3/n_3c\epsilon_0} a_3.$$

The coupled-mode equations for the normalized field amplitudes (under phase-matched conditions) can be written in the form

$$\frac{da_1}{dz} = \kappa a_3 a_2 \quad (5)$$

$$\frac{da_2}{dz} = \kappa a_3 a_1 \quad (6)$$

$$\frac{da_3}{dz} = -\kappa a_1 a_2 \quad (7)$$

where the coupling constant is defined as

$$\kappa = d_e \sqrt{\frac{2\hbar}{c^3\epsilon_0}} \sqrt{\frac{\omega_1\omega_2\omega_3}{n_1n_2n_3}}. \quad (8)$$

In the case of second-harmonic generation (SHG), one has the fundamental field at $\omega = \omega_1 = \omega_2$ and the second-harmonic field at $2\omega = \omega_3$. Depending on the type of phase matching that is utilized, a_1 and a_2 may or may not be distinguishable from each other. In type-I phase matching, the two fields are degenerate in every aspect and are indistinguishable. This degeneracy reduces the number of coupled mode equations to two [10]:

$$\frac{da_4}{dz} = -\kappa a_6 a_4 \quad (9)$$

$$\frac{da_6}{dz} = \frac{1}{2} \kappa a_4^2 \quad (10)$$

with the coupling constant

$$\kappa = d_e \sqrt{\frac{2\hbar}{c^3\epsilon_0}} \sqrt{\frac{2\omega^3}{n_4n_5n_6}} \quad (11)$$

where a_4 is the fundamental at ω , a_6 is the second-harmonic at 2ω , and $n_4 = n_5$. As in the OPA case, the lack of a second-harmonic field at the input allows us to write the coupled-mode equations for real field amplitudes, where $E_4 = \sqrt{2\hbar\omega_4/n_4c\epsilon_0} a_4$ and $E_6 = -j\sqrt{2\hbar\omega_6/n_6c\epsilon_0} a_6$. In type-II phase matching, a_1 and a_2 have orthogonal polarizations and, thus, are nondegenerate in polarization. The coupled-mode equations for this case are

$$\frac{da_4}{dz} = -\kappa a_6 a_5 \quad (12)$$

$$\frac{da_5}{dz} = -\kappa a_6 a_4 \quad (13)$$

$$\frac{da_6}{dz} = \kappa a_4 a_5 \quad (14)$$

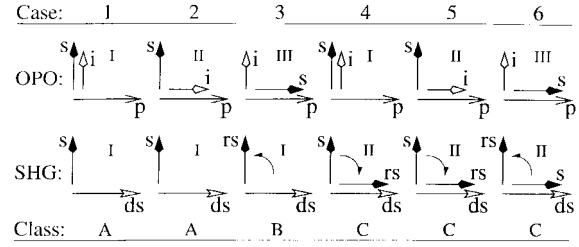


Fig. 1. Polarization diagrams for all possible self-doubling geometries. The fast axis is horizontal and the slow axis is vertical. Polarizations for the pump (p), signal (s), idler (i), polarization rotated signal (rs), and frequency-doubled signal (ds) are shown. Intracavity polarization rotation is indicated with an arc where required.

TABLE I
POTENTIAL PHASE-MATCHING GEOMETRIES FOR THE SELF-DOUBLING OPO

Type	OPO		SHG	
	$\omega_3 \rightarrow \omega_1 + \omega_2$	$\omega_2 + \omega_2 \rightarrow 2\omega_2$		
I	$f \rightarrow s + s$	$s + s \rightarrow f$		
II	$f \rightarrow f + s$	$s + f \rightarrow f$		
III	$f \rightarrow s + f$			

Case	OPO	SHG	Rotation	Class
1	I	I	no	A
2	II	I	no	A
3	III	I	yes	B
4	I	II	yes	C
5	II	II	yes	C
6	III	II	yes	C

Normal dispersion is assumed. The fast and slow axes are denoted by f and s , respectively.

where a_4 and a_5 are the orthogonally polarized components of the fundamental at ω and a_6 is the second-harmonic at 2ω . Ordinarily, maximum conversion to the second-harmonic takes place if the two orthogonal polarizations have the same photon flux density. Therefore, the usual practice is to orient a linearly polarized fundamental field at a 45° angle to the two eigen-polarization directions.

III. THE SELF-DOUBLING OPO

The self-doubling OPO is based on the premise that both parametric generation and frequency doubling can be phase matched for the same direction of propagation inside the nonlinear crystal. This may happen in a number of different polarization geometries, depending on the types of OPO and SHG phase matching. Some of these geometries require an intracavity polarization rotation for the signal field while others do not.

Table I and Fig. 1 together summarize all polarization geometries that can potentially be phase matched for a self-doubling OPO. We follow the convention that the fields are labeled according to $\omega_1 < \omega_2 < \omega_3$ [13]. The field at ω_3 is

the OPO pump, since this is the highest frequency OPO field. The assignment of the “signal” label to ω_1 or ω_2 is somewhat arbitrary. In this paper, the resonant field in the OPO cavity, which also constitutes the fundamental field for the SHG process, is called the “signal.” For frequency upconversion with the self-doubling OPO, the signal field has to be at ω_2 , so that $2\omega_2 > \omega_3$ can be satisfied.

For materials exhibiting normal dispersion, the highest frequency fields of both interactions (ω_3 and $2\omega_2$) have to be polarized along the fast axis of the crystal. In a type-I OPO, both the signal and the idler are polarized along the slow axis, whereas in a type-II (III) OPO, the signal is along the slow (fast) axis and the idler is along the fast (slow) axis. Type-I SHG has the fundamental along the slow axis, whereas type-II SHG has a fundamental component along both the fast and the slow axes. There is no type-III interaction for SHG since this process is degenerate in frequency.

There are six possible cases corresponding to different combinations of phase-matching types for the OPO and SHG, as shown in Table I and Fig. 1. For each case, the respective coupling constants κ_a and κ_b that govern the parametric and second-harmonic processes depend on the phase-matched frequencies, the refractive indices, and the effective nonlinear coefficients. The ratio of the two coupling constants $\beta = \kappa_b/\kappa_a$ is an important quantity that may assume a range of values depending on these parameters. Here, the relative magnitudes of the frequencies and effective nonlinear coefficients are of particular importance. If the OPO and SHG processes are of the same phase-matching type (cases 1, 5, and 6), the effective nonlinear coefficients differ only due to dispersion [13]. However, for different phase-matching types (cases 2–4) the effective nonlinear coefficients may be dramatically different from each other, since they have different functional dependences on the elements of the second-order nonlinear tensor.

In cases 1 and 2, the polarization of the OPO signal is the same as that of the SHG fundamental. As a result, the signal field is common to the OPO and SHG processes, which become coupled to each other through the signal field. The set of coupled mode equations that describe this interaction are

$$\frac{da_1}{dz} = \kappa_a a_3 a_2 \quad (15)$$

$$\frac{da_2}{dz} = \kappa_a a_3 a_1 - \kappa_b a_6 a_2 \quad (16)$$

$$\frac{da_3}{dz} = -\kappa_a a_1 a_2 \quad (17)$$

$$\frac{da_6}{dz} = \frac{1}{2} \kappa_b a_2^2 \quad (18)$$

where κ_a and κ_b are the coupling constants for the parametric generation and second-harmonic generation processes, respectively. We arrive at these equations by combining the OPO equations [(5)–(7)] with the type-I SHG equations [(9)–(10)]. The signal a_2 and the fundamental a_4 are the same field mode; the rate of change of this mode is the sum of the rates of change of the signal and the fundamental fields separately. The same result can be obtained by considering the total nonlinear polarization field P_2 at ω_2 and rederiving the coupled-mode

equations. Note that the only difference between cases 1 and 2, other than possibly having different β values, is the polarization direction of the idler, which is irrelevant to the self-doubling process. Therefore, the same set of coupled mode equations govern both cases. We designate this self-doubling OPO process as class A.

In case 3, the polarization of the OPO signal is orthogonal to that of the SHG fundamental. However, an intracavity polarization rotation allows the same crystal to be used for both processes at the same time. During each round trip in the cavity, the polarization of the signal field is rotated by a certain amount, resulting in an additional linear loss for the linearly polarized signal mode, but creating a field component for the SHG fundamental. However, the two processes are not coupled in the crystal as they are in class-A interactions, and the coupled-mode equations that govern this self-doubling OPO are simply (5)–(7) and (9)–(10). We designate this self-doubling OPO as class B.

In cases 4–6, SHG is a type-II process, requiring a fundamental field along both the fast and the slow axes. The OPO signal is common to either one or the other of these two components, regardless of the type of OPO phase matching. As a result, the two processes are coupled to each other through the signal field, as in class-A self-doubling OPO’s. However in the present case, the coupling is through only one polarization component of the fundamental. An intracavity polarization rotation of the signal field is required for SHG to take place. The set of coupled mode equations that describe all three cases are

$$\frac{da_1}{dz} = \kappa_a a_3 a_2 \quad (19)$$

$$\frac{da_2}{dz} = \kappa_a a_3 a_1 - \kappa_b a_6 a_5 \quad (20)$$

$$\frac{da_3}{dz} = -\kappa_a a_1 a_2 \quad (21)$$

$$\frac{da_5}{dz} = -\kappa_b a_6 a_2 \quad (22)$$

$$\frac{da_6}{dz} = \kappa_b a_2 a_5. \quad (23)$$

We designate this self-doubling OPO process as class C. The only difference between cases 4 and 5 is the polarization direction of the idler. In case 6, the polarization direction of the signal and the rotated signal are interchanged (with respect to those in cases 4 and 5), but this makes no difference in the equations since the SHG process is symmetric to this change.

In ordinary three-wave mixing, as described by (5)–(7), Manley–Rowe relations state that the quantities $(\phi_1 + \phi_3)$ and $(\phi_2 + \phi_3)$ are conserved throughout the interaction [10]. It is possible to formulate similar conservation laws for the self-doubling OPO’s. For class-A OPO’s, the quantities $(\phi_1 + \phi_3)$ and $(\phi_2 + \phi_3 + 2\phi_6)$ are conserved. Similarly, for class-C OPO’s, the quantities $(\phi_1 + \phi_3)$, $(\phi_2 + \phi_3 + \phi_6)$, and $(\phi_5 + \phi_6)$ are conserved.

IV. SOLUTIONS

In order to analyze the performance of self-doubling OPO’s, it is necessary to calculate the single-pass saturated parametric

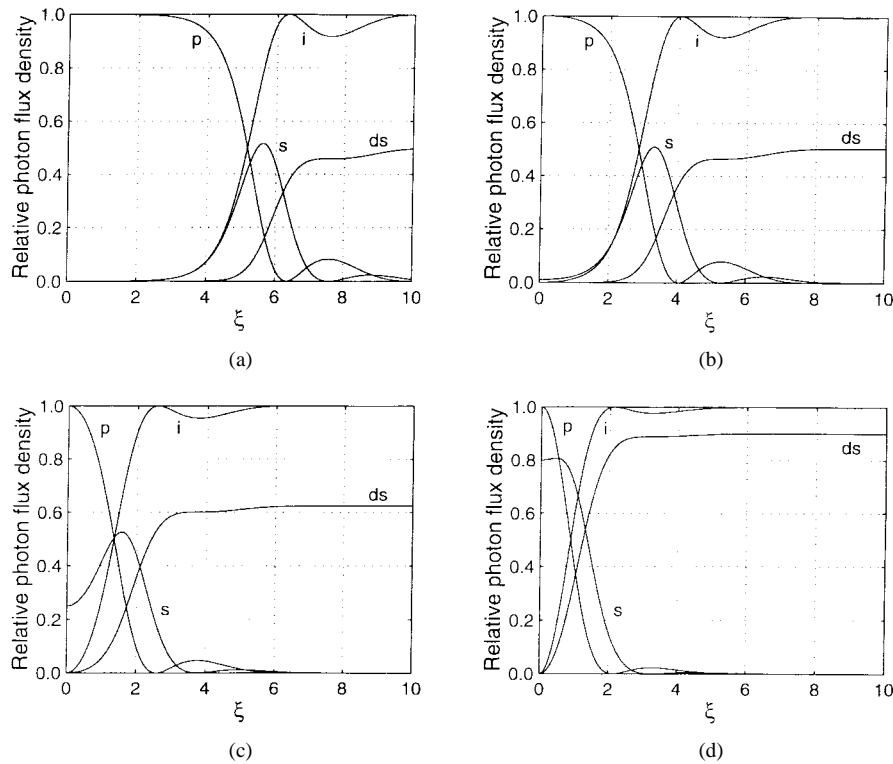


Fig. 2. Single-pass solutions for a class-A self-doubling OPA for different input signal photon flux densities $\phi_2(0)$. (a) $10^{-4}\phi_3(0)$. (b) $10^{-2}\phi_3(0)$. (c) $0.25\phi_3(0)$. (d) $0.8\phi_3(0)$. The evolution of the pump (p), signal (s), idler (i), and frequency-doubled signal (ds) fields are shown as functions of the normalized propagation distance ξ in the crystal. In all cases $\beta = 1.5$. All fields are shown normalized to the input pump flux.

gain experienced by the signal field. Analytical solutions of class-B equations are readily available in the form of OPA and SHG solutions separately, since the two processes are not coupled in the crystal. These are the well-known OPA and SHG solutions in terms of Jacobi elliptic functions [11] and hyperbolic functions [10], respectively. For class-A and class-C self-doubling OPO's, however, we resorted to numerical techniques to solve the coupled mode equations. These solutions were computed using forward finite differencing and variable step Runge–Kutta integration. These two methods were implemented independently to verify the results against each other.

We first used forward finite differencing of complex field amplitudes to compute the evolution of the fields in a single pass through the nonlinear crystal. We found that the single-pass solutions of complex class-A and class-C coupled-mode equations are phase insensitive if no idler or second-harmonic is present at the crystal input. This expected behavior justifies our converting the complex coupled-mode equations to real equations. We solved the set of real equations using the Runge–Kutta–Fehlberg method, and verified these solutions with our previous results obtained from finite differencing of complex field amplitudes.

In our calculations, the order of magnitude of most physical parameters are either based on the experiment reported by Kartaloğlu *et al.* [9], or some estimate as to what range of values they are more likely to be in. However, our aim here is not to model this experiment accurately, but to bring out the fundamental properties of self-doubling OPO's using a simple continuous-wave monochromatic plane-wave theory.

Our analysis does not take into account many experimental realities such as the Gaussian beam nature of the fields, the temporal profile of the pulses, group velocity mismatch between field components, group velocity dispersion, or beam walk-off.

A. Class-A Self-Doubling OPO's

Fig. 2 shows single-pass solutions for a specific class-A self-doubling OPA as an example. The evolution of the photon flux densities for the pump, signal, idler, and frequency-doubled signal fields along the direction of propagation inside the crystal are shown for different levels of signal input. We follow convention and define a dimensionless normalized propagation distance $\xi = \kappa_a a_3(0)z$ to present the results more generally [6]. For this example, we have taken $\beta = 1.5$. All photon flux densities are normalized to the input pump photon flux density $\phi_3(0) = a_3^2(0)$.

In Fig. 2(a), the input signal flux is $\phi_2(0) = 10^{-4}\phi_3(0)$. We observe that for low input signal flux levels like this, the OPA process dominates the interaction at smaller values of ξ . In this region, the signal experiences gain without much saturation. The pump is depleted by 10% at $\xi = 4.2$. There is not much SHG up to this point [$\phi_6 = 1.5 \times 10^{-3} \phi_3(0)$], since the signal flux is not high enough for efficient conversion. However, the SHG process begins to show its influence at larger values of ξ , as the signal flux further increases. This increase becomes more gradual because of gain saturation (pump depletion) and conversion to the second-harmonic, and reaches a maximum at $\xi = 5.6$. At this point, the pump is depleted by 79.5%

and the second-harmonic flux is 14.0% of the input pump flux. From then on, the signal decreases due to SHG, but still draws energy from the pump. The pump is fully depleted at $\xi = 6.3$, after which there is a small amount of backconversion of the signal and the idler to the pump. The pump flux reaches 8.2% of its value at the input and then begins to decrease again, with a corresponding increase in the signal and idler flux. At some point $\xi > 10$, the pump is fully depleted again. However, this oscillatory ringing behavior dies out and the interaction stops, the entire pump being converted to the idler and the second-harmonic. Neglecting the contribution of the input signal, for every two pump photons at the input, there are two idler photons and one second-harmonic photon at the output.

Increasing the input signal flux [to $10^{-2}\phi_3(0)$ in Fig. 2(b)] shifts the entire process in the negative ξ direction. The evolution of the field components are not altered in any appreciable way until the input signal level increases to a value that is a significant fraction of the pump. Fig. 2(c) shows the evolution of the fields for an input signal flux of $0.25\phi_3(0)$. We observe that the SHG process starts drawing energy from the signal right away. Also, the ringing behavior due to backconversion gets smaller in amplitude with increasing input signal flux. When the input signal level is increased further [to $0.8\phi_3(0)$ in Fig. 2(d)], the SHG process dominates the interaction from the beginning. For an input signal flux exceeding 89% of the input pump flux, the signal flux decreases monotonically for all values of ξ .

The parameter β is a measure of the prominence of the SHG process over the OPA process. Its value is an important factor influencing the behavior of the solutions. With decreasing β , the effect of SHG becomes less, and the ringing behavior due to the OPA process increases in amplitude, total conversion to the second-harmonic occurring farther in the crystal. Increasing β has the opposite effect of decreasing the ringing behavior.

For a fixed crystal length (l), the gain of an ordinary OPA is fully characterized by the dimensionless parameter $(\kappa_a l)^2 \phi_3(0)$, called the nonlinear drive [6], [7]. However, in a self-doubling OPO, the net gain experienced by the signal field is clearly influenced by both the OPA and SHG processes. Fig. 3 shows the net parametric gain g as a function of the input signal flux [normalized to the input pump flux $\phi_3(0)$] for various values of β , while the nonlinear drive is fixed at a value of 1. The unsaturated (small-signal) gain is independent of β , and has a value of 2.38 (3.77 dB) for the given nonlinear drive. The gain decreases from this value as the input signal flux is increased, and eventually becomes less than unity (0 dB) for nonzero β . This behavior is in stark contrast to an ordinary OPA ($\beta = 0$), which never has a gain that is less than unity and saturates more gradually with increasing signal input.

A singly resonant self-doubling OPO is constructed by placing the nonlinear crystal inside a cavity that is resonant at the signal frequency. The pump field enters the cavity through a dichroic mirror that is highly transmissive at that wavelength. The cavity will typically have a few percent of linear loss (L) due to less than unity reflectivities of the cavity mirrors, imperfect antireflection coatings on the nonlinear crystal, and

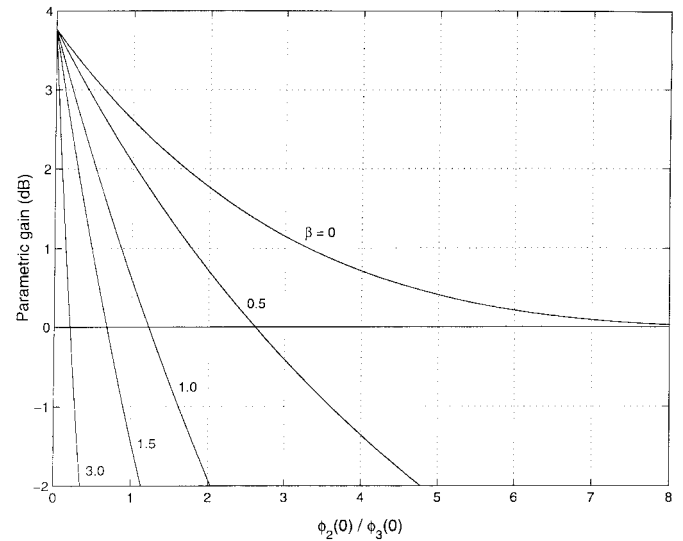


Fig. 3. Saturation of parametric gain with input signal flux $\phi_2(0)$ in class-A self-doubling OPA's for various values of β at a fixed nonlinear drive of 1.

other transmissive optics. Oscillation starts if the unsaturated gain is higher than the total cavity losses. The intracavity signal flux assumes such a value that the saturated gain compensates for the cavity losses exactly. This intracavity signal flux is found by solving

$$g[\phi_2(0)] = \frac{1}{1-L} \quad (24)$$

numerically for $\phi_2(0)$. This is equivalent to finding the intersection of the gain saturation curve of Fig. 3 with a horizontal line of value $1/(1-L)$ (in decibels). Once the signal flux at the input of the crystal is known, all other fields can be calculated using single-pass solutions.

In our calculations, we take the total cavity loss L to be 4%. For this value, the signal flux at the input of the crystal is found to be $0.644\phi_3(0)$ (with a nonlinear drive of 1 and $\beta = 1.5$). Fig. 4 shows the evolution of the fields inside the crystal as a function of the normalized propagation distance under these circumstances. All fields are shown normalized to the input pump photon flux. The signal flux starts from 64.4%, goes through a maximum of 69.3%, and then at the output facet decreases to 67.0% of the input pump flux, experiencing a net gain of 1.042. The second-harmonic flux at the output of the crystal is 25.4% of the input pump flux. The second-harmonic is readily coupled out of the cavity with the use of a dichroic cavity mirror that is highly transmissive at this wavelength. The pump is depleted by 53.4%; and the output idler field, which is also coupled out of the cavity with a dichroic mirror, has a photon flux that is 53.4% of the input pump flux.

The performance of the self-doubling OPO is characterized by the photon conversion efficiency, the ratio of twice the output second-harmonic flux to the input pump flux, $2\phi_6(l)/\phi_3(0)$, since two pump photons are needed to generate one second-harmonic photon. The conversion efficiency represents the overall efficiency of the two-step process from the pump to the signal to the second-harmonic, and is equal to unity for the case of total conversion. The nonlinear drive along with β uniquely determine the conversion efficiency of

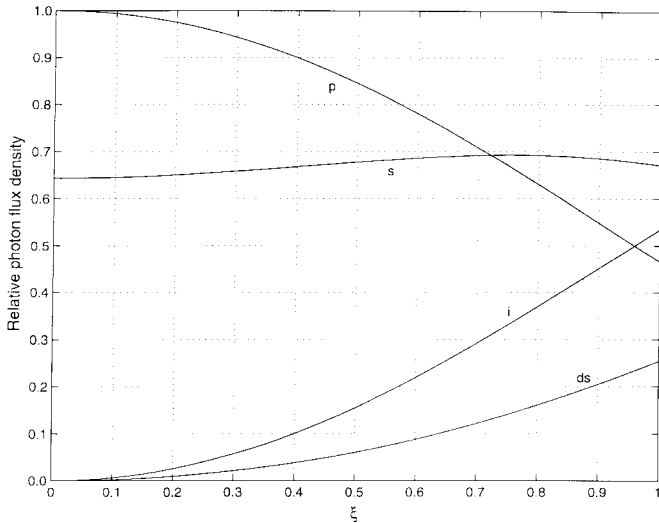


Fig. 4. Evolution of the pump (p), signal (s), idler (i), and frequency-doubled signal (ds) fields as functions of the normalized propagation distance ξ in the crystal for a class-A self-doubling OPO. The nonlinear drive is 1, $\beta = 1.5$, and linear cavity losses are taken to be 4%. All fields are shown normalized to the input pump flux.

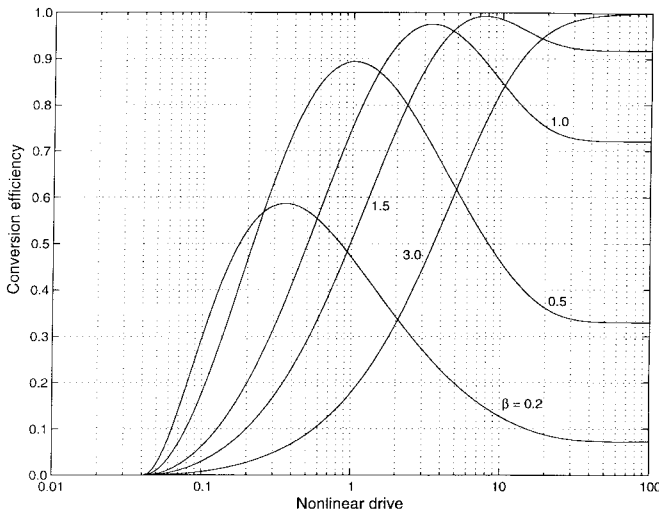


Fig. 5. Conversion efficiency as a function of the nonlinear drive for class-A self-doubling OPO's for various values of β .

the self-doubling OPO. Fig. 5 shows the dependence of the conversion efficiency on the nonlinear drive for various values of β for a fixed cavity loss of 0.04. The threshold nonlinear drive of this self-doubling OPO is 0.041 and independent of β . (This is equal to the threshold nonlinear drive of an ordinary OPO with a signal output coupler reflectivity of $R = 1 - L = 0.96$.) Note that the conversion efficiency is very high for a large range of the nonlinear drive, provided β is not small ($\beta \geq 1.0$).

Fig. 6 shows the nonlinear drive dependence of the ratio of the intracavity signal flux to the input pump flux for various values of β . With increasing nonlinear drive, the ratio of intracavity signal to the input pump increases first, reaches a maximum, and starts decreasing after that. At a fixed value of the nonlinear drive, a larger β results in a smaller intracavity signal flux. This behavior is a result of the nonlinear output

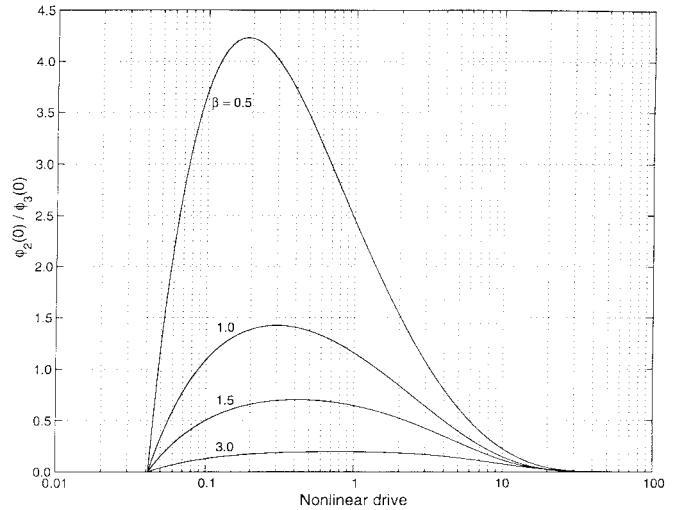


Fig. 6. Intracavity signal flux (normalized to the input pump flux) as a function of the nonlinear drive for class-A self-doubling OPO's for various values of β .

coupling mechanism through the SHG process and can also be observed in Fig. 3. It is interesting to note that the intracavity signal flux is always less than the input pump flux when β is larger than 1.23.

We observe that near-quantum-limited wavelength upconversion is possible using a class-A self-doubling OPO. Even though there is an optimum nonlinear drive for a particular value of β , variations from this optimum have little effect if β is high (≥ 1 , for example). This indicates that pulsed self-doubling OPO's pumped with beams having transverse intensity variations are also likely to be efficient devices. However, the optimum nonlinear drive required by interactions having a large β value may be difficult to attain. Low intracavity signal flux levels reduce the risk of exceeding the damage threshold of the nonlinear crystal in pulsed applications.

B. Class-B Self-Doubling OPO's

In class-B self-doubling OPO's, the OPA and SHG processes are independent of each other, since the OPA signal and the SHG fundamental have orthogonal polarizations. However, an intracavity polarization rotation of the signal field with the use of a half-wave retarder can couple the two processes and allow frequency doubling to take place. For an intracavity polarization rotation angle of α , a $\sin^2 \alpha$ fraction of the signal flux is coupled to the fundamental field mode. Consequently, the signal field mode experiences an additional linear loss of $\sin^2 \alpha$. At each pass through the crystal, the signal experiences parametric gain, whereas the fundamental gets converted to the second-harmonic. Here, we assume that the residual fundamental at the output of the crystal is either coupled out of the cavity with the use of a polarizing beamsplitter, or negligible due to strong conversion. If instead both the signal and the fundamental fields are resonated in the OPO cavity, the polarization mixing at the retarder will result in the interference of the two fields in an uncontrolled fashion.

As far as the OPO signal is concerned, the situation at hand is the same as an ordinary OPO with an output coupler

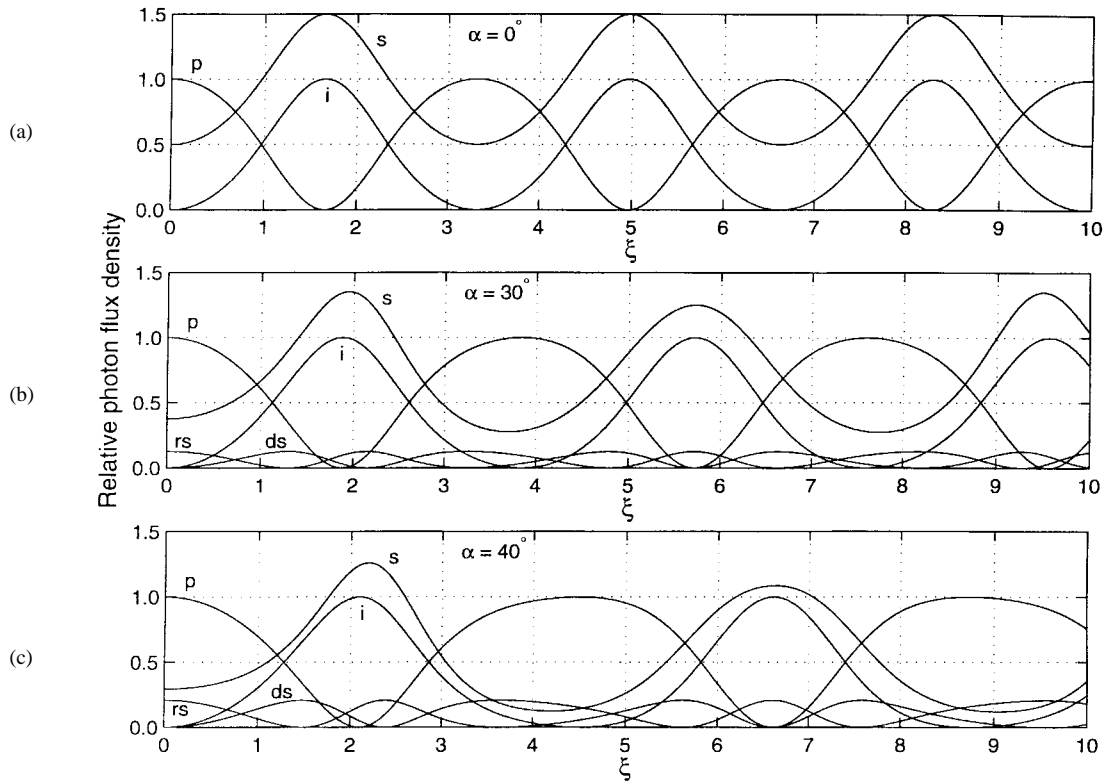


Fig. 7. Single-pass solutions for a class-C self-doubling OPA for different polarization rotation angles α : (a) 0° , (b) 30° , and (c) 40° . The evolution of the pump (p), signal (s), idler (i), polarization rotated signal (rs), and frequency-doubled signal (ds) photon flux densities are shown as functions of the normalized propagation distance ξ in the crystal. The total input flux at the signal wavelength is $0.5\phi_3(0)$ and $\beta = 1.67$ in all cases. All fields are shown normalized to the input pump flux.

reflectivity of $R = \cos^2 \alpha$. The OPO signal experiences a total linear loss of

$$L = 1 - (1 - L_c) \cos^2 \alpha \quad (25)$$

where L_c is the collective cavity loss due to less than unity reflectivities of the mirrors and imperfect antireflection coatings on the nonlinear crystal and other transmissive optics such as the wave retarder and the polarizing beamsplitter. There is no nonlinear output coupling in this situation, and the intracavity signal flux is solely determined by the polarization rotation angle α and residual cavity losses L_c . Even though the SHG process is internal to the OPO cavity, it does not benefit from high values of the intracavity signal flux. In effect, this configuration is not different from external frequency doubling of an ordinary OPO. As such, it is not expected to be particularly efficient.

On the other hand, a different mode of operation is achieved if the residual fundamental is not coupled out and the polarization rotation angle α is set to 90° . In this situation, the retarder switches around the polarizations of the signal and the residual fundamental, with no resulting interference due to polarization mixing. The signal at the output of the crystal provides the fundamental for SHG for the next round trip, whereas the residual fundamental becomes the OPA input. Since the two processes are not coupled in the crystal, this configuration is conceptually equivalent to intracavity frequency doubling of an ordinary OPO with a second crystal. The plane-wave

theory of such two crystal intracavity-doubled OPO's has been analyzed elsewhere previously [7].

C. Class-C Self-Doubling OPO's

Class-C self-doubling OPO's are characterized by a type-II phase-matched SHG process, where the fundamental is composed of two orthogonally polarized field modes. The polarization of the OPO signal mode coincides with one of these fundamental modes regardless of the type of OPO phase matching. Since in principle there will be no SHG if both fundamental polarizations are not present, a rotation of the signal polarization inside the OPO cavity with the use of a half-wave retarder is required to achieve frequency doubling.

In calculating the single-pass solutions of class-C coupled-mode equations, we take the total linearly polarized input flux at the signal (and fundamental) wavelength to be ϕ_t . We then rotate the polarization of this input field by α degrees such that the input signal flux is $\phi_t \cos^2 \alpha$, and the input rotated signal (fundamental) flux is $\phi_t \sin^2 \alpha$. Fig. 7 shows single-pass solutions for a specific class-C self-doubling OPA for three different values of the polarization rotation angle α . For this example, we have taken $\phi_t = 0.5\phi_3(0)$ and $\beta = 1.67$. The rotation angle α is set to zero for the solutions shown in Fig. 7(a). Since there is no polarization rotation, only one of the two orthogonally polarized fundamental field components is present at the input. The numerical solutions for the evolution of the signal, idler, and pump fields reproduce

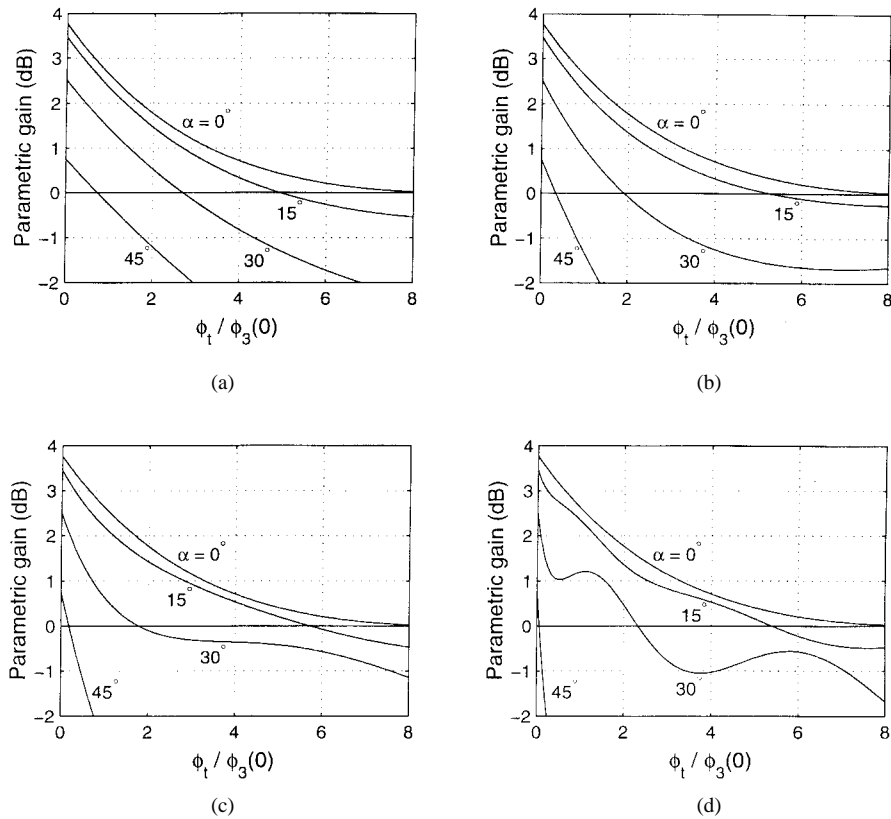


Fig. 8. Saturation of parametric gain with total input flux ϕ_t in class-C self-doubling OPA's for various values of the polarization rotation angle α and the ratio of coupling constants β . (a) $\beta = 0.5$. (b) $\beta = 1.0$. (c) $\beta = 1.5$. (d) $\beta = 3.0$. The nonlinear drive is 1 in all cases.

the same well-known periodic solutions for an ordinary OPA in terms of Jacobi elliptic functions [11].

Fig. 7(b) and (c) shows the evolution of the fields for polarization rotation angles of 30° and 40° , respectively. We observe that even though the evolution of the fields along the direction of propagation is still oscillatory, polarization rotation seems to destroy the periodic behavior seen in an ordinary OPO ($\alpha = 0^\circ$). Furthermore, the minima and maxima of various field modes do not occur at the same point in ξ either. The minima (maxima) of the second-harmonic coincide with the maxima (minima) of the rotated signal; and the minima (maxima) of the idler coincide with the maxima (minima) of the pump, in accordance with the conservation laws. However, the minima and maxima of the signal do not coincide with the minima or maxima of any other field.

We have taken $\beta = 1.67$ in this example to illustrate the seemingly nonperiodic behavior of the solutions. The Manley–Rowe conserved quantities $C_1 = a_1^2 + a_3^2$, $C_2 = a_2^2 + a_3^2 + a_6^2$, and $C_3 = a_5^2 + a_6^2$ allow us to derive a fourth conserved quantity and gain further insight into the β dependence of the solutions. It is possible to make the transformations $a_1 = \sqrt{C_1} \sin \theta$, $a_3 = \sqrt{C_1} \cos \theta$, $a_5 = \sqrt{C_3} \cos \gamma$, and $a_6 = \sqrt{C_3} \sin \gamma$, and substitute into (19) and (23) to get

$$a_2 = \frac{1}{\kappa_a} \frac{d\theta}{dz} = \frac{1}{\kappa_b} \frac{d\gamma}{dz}. \quad (26)$$

When integrated, this equation yields a fourth conserved quantity $C_4 = \theta/\kappa_a - \gamma/\kappa_b$, which is equal to zero since

no idler or second-harmonic is present at the crystal input. Using this relation and the Manley–Rowe relation for C_2 , we can reduce the coupled-mode equations to a single differential equation

$$\frac{1}{\kappa_a^2} \left(\frac{d\theta}{dz} \right)^2 + C_1 \cos^2(\theta) + C_3 \sin^2(\beta\theta) = C_2 \quad (27)$$

in the variable $\theta(z)$. If $C_1 \cos^2(\theta) + C_3 \sin^2(\beta\theta)$ can be larger than C_2 for any value of θ (which may be possible only if $\alpha > 45^\circ$), the solution of (27) oscillates periodically around zero. Otherwise, $\theta(z)$ increases monotonically; the solution is periodic only if β has a rational value, and aperiodic otherwise. If $\beta = p/q$ (p and q being integers), then the pump (idler) goes through q number of minima (maxima), and the rotated signal (second-harmonic) goes through p number of minima (maxima), in a single period of the solutions. Unless both p and q are small integers, this periodic character cannot be observed in just a few cycles of pump depletion and backconversion.

For a fixed value of β , the value of the polarization rotation angle α determines the degree of coupling between the OPA and the SHG processes. As the signal field propagates through the crystal, it experiences amplification due to parametric generation and nonlinear loss due to SHG. The nonlinear SHG loss depends on the photon flux density of the orthogonally polarized fundamental mode, as well as the signal flux itself. Furthermore, as far as the field component at the signal polarization is concerned, polarization rotation results in an additional $\sin^2 \alpha$ linear loss factor. Therefore, we define the net gain, including the effect of polarization rotation, as the ratio

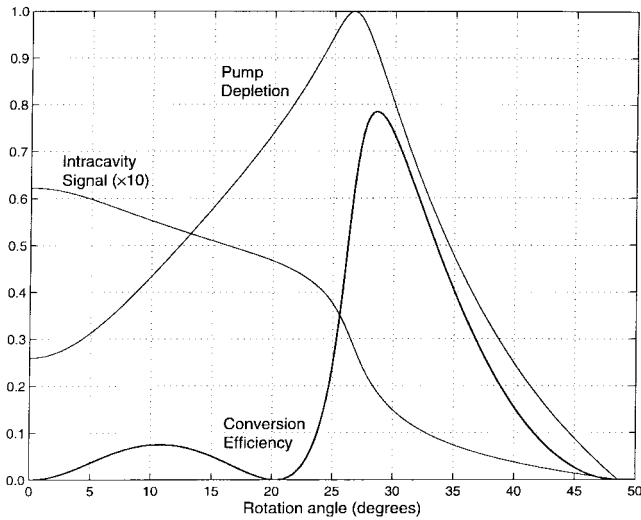


Fig. 9. Conversion efficiency, pump depletion, and intracavity signal flux (normalized to the input pump flux), as functions of polarization rotation angle α in a class-C self-doubling OPO. The nonlinear drive is 1 and $\beta = 1.5$.

of the output signal flux to the total input flux; $g = \phi_2(l)/\phi_t$. We assume that the rotated signal component at the output is either separated from the signal component with the use of a polarizing beamsplitter, or strongly depleted.

Fig. 8 shows the net gain as a function of the total input flux (normalized to the input pump flux) for different values of α and β at a fixed nonlinear drive of 1. For $\alpha = 0^\circ$, regardless of the value of β , we have an ordinary OPA with a small-signal gain of 2.38 (3.77 dB) that saturates with increasing input flux and reaches unity around $\phi_t = \phi_2(0) \approx 8\phi_3(0)$. When α is increased, the unsaturated gain decreases as $\cos^2 \alpha$, because of the extra linear loss that the signal field experiences. The saturation behavior of the gain depends on the value of β . For smaller values of β , saturation is monotonic and more rapid with increasing α . Larger values of β show more erratic behavior, with regions of very gradual saturation and even nonmonotonic character.

The intracavity signal flux for a class-C self-doubling OPO at a constant value of α is found by solving (24) using the net gain shown in Fig. 8. Since the linear loss induced by the polarization rotation is already included in the solution for the net gain, L represents all other linear cavity losses. Fig. 9 shows the dependence of the intracavity signal flux, conversion efficiency, and pump depletion to the polarization rotation angle α at a constant nonlinear drive of 1, $\beta = 1.5$, and $L = 0.04$. The conversion efficiency starts out from zero at $\alpha = 0^\circ$, increases to 7.5% at $\alpha = 10.7^\circ$, and becomes zero again at $\alpha = 20.3^\circ$. Thereafter, the conversion efficiency increases very rapidly to reach a maximum value of 78.5% at $\alpha = 28.6^\circ$, and decreases again until the OPO goes below the threshold at $\alpha = 48.6^\circ$. On the other hand, the pump depletion starts at 27% at $\alpha = 0^\circ$ and increases to unity at $\alpha = 26.6^\circ$, and then decreases as α is increased further. It is interesting to note that maximum conversion does not occur at the same α as that for complete pump depletion. The intracavity signal level is 6.2 times the input pump flux at $\alpha = 0^\circ$ and decreases monotonically with increasing α . The OPO threshold is 4.1%

of the nonlinear drive at $\alpha = 0^\circ$ and increases with α because of the extra linear losses induced by polarization rotation.

Fig. 10 shows the evolution of the fields at four different values of α , for a nonlinear drive of 1, $\beta = 1.5$, and $L = 0.04$. All fields are shown as normalized to the input pump photon flux. Fig. 10(a) corresponds to the first smaller peak of the conversion efficiency at $\alpha = 10.7^\circ$ in Fig. 9. We observe that the second-harmonic goes through a maximum at $\xi = 0.44$ inside the crystal, at which point the rotated signal is fully depleted. The pump is fully depleted at $\xi = 0.66$ but increases after that due to backconversion. The second-harmonic also goes through a zero, which occurs at $\xi = 0.87$, and then at the output increases to 3.8% of the input pump flux.

Fig. 10(b) shows the evolution of the fields at $\alpha = 20.3^\circ$, the angle at which conversion to the second-harmonic is zero. We observe that the evolution of the fields has in general shifted in the positive ξ direction, and their amplitudes have changed considerably. The pump is fully depleted at $\xi = 0.76$, and the doubled signal reaches a maximum at $\xi = 0.53$ before decreasing to zero at the crystal output. In Fig. 10(c), α is set to 26.6° , the angle at which full pump depletion occurs. The second-harmonic goes through its maximum at $\xi = 0.69$, and decreases to 29.4% of the input pump flux at the output. Note that a significant amount of rotated signal flux is present at the output of the crystal. This flux is wasted since it is coupled out of the cavity.

Fig. 10(d) corresponds to $\alpha = 28.6^\circ$, the angle at which there is maximum conversion to the second-harmonic. The second-harmonic goes through a maximum at $\xi = 0.85$ inside the crystal and decreases to 39.2% of the input pump flux at the output. The pump depletion for this case is 90.6%. We note that the amount of polarization rotation is critical for the efficient operation of class-C self-doubling OPO's. In a practical device, α can easily be adjusted to its optimum value by rotating the intracavity half-wave retarder.

Fig. 11 shows the dependence of the conversion efficiency and pump depletion on the nonlinear drive for different values of β . For each β , the rotation angle α is adjusted to optimize the conversion efficiency at a fixed nonlinear drive of 1. This α is kept fixed as the nonlinear drive is increased to generate the curves of Fig. 11. Naturally, maximum conversion efficiency occurs at a nonlinear drive very close to 1. However, the conversion efficiency drops from its maximum value relatively quickly as the nonlinear drive is changed, in contrast to class-A self-doubling OPO's (see Fig. 5). This sensitivity to the nonlinear drive increases with increasing β .

The intracavity signal flux and consequently the conversion efficiency and pump depletion show discontinuities in their nonlinear drive dependence at large values of β . An example of this is seen in Fig. 11(d) for $\beta = 3$. This behavior is a consequence of the nonmonotonic behavior of the gain saturation curve such as the one shown in Fig. 8(d). In general, (24) can have multiple solutions, depending on the values of the nonlinear drive, α , and β . In Fig. 11, we always choose the smallest of these solutions, assuming that the intracavity signal builds up from noise to reach its steady-state value. However, a hysteresis behavior can be observed in the intracavity signal flux if the nonlinear drive is varied up and down.

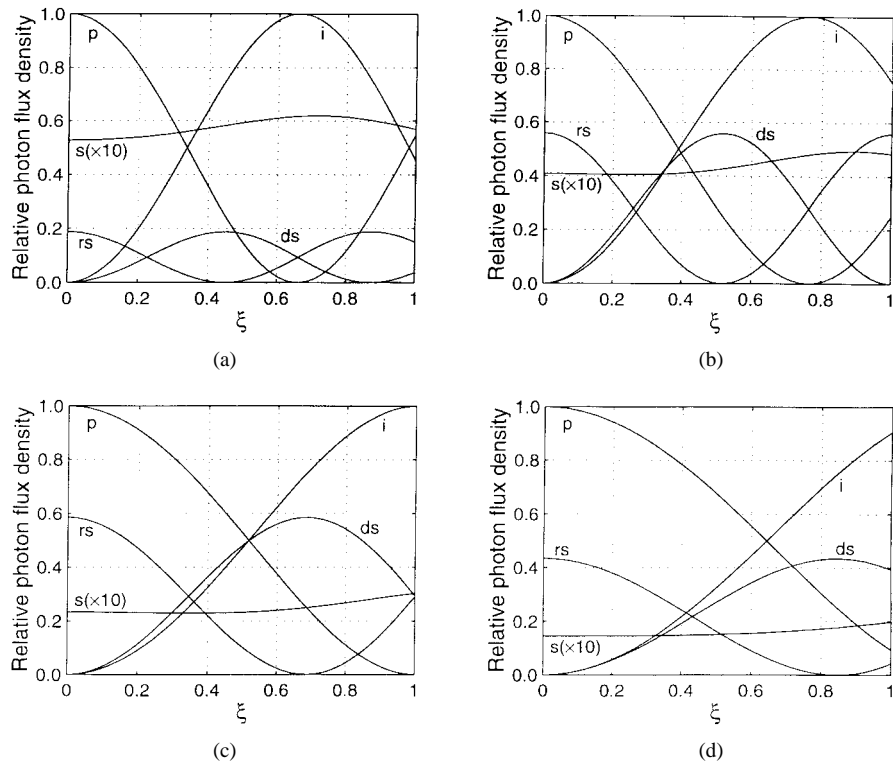


Fig. 10. Evolution of the pump (p), signal ($s \times 10$), rotated signal (rs), idler (i), and doubled signal (ds) fields in the crystal, for different values of the polarization rotation angle α for a class-C self-doubling OPO: (a) $\alpha = 10.7^\circ$, (b) $\alpha = 20.3^\circ$, (c) $\alpha = 26.6^\circ$, and (d) $\alpha = 28.6^\circ$. The nonlinear drive is 1 and $\beta = 1.5$ in all cases.

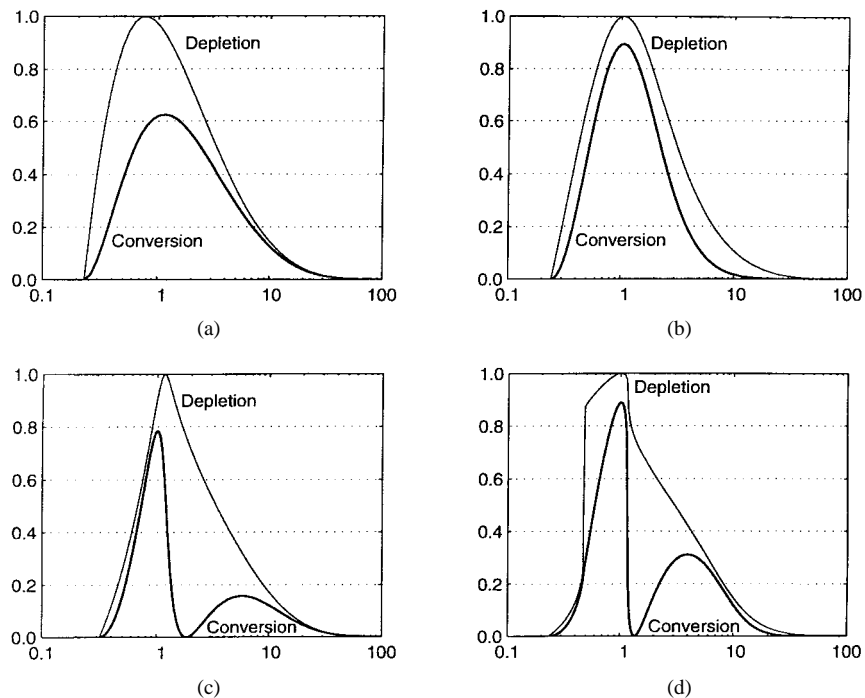


Fig. 11. Conversion efficiency and pump depletion as functions of the nonlinear drive for class-C self-doubling OPO's for different values of β . For each β value, the rotation angle α is adjusted to maximize the conversion efficiency at a nonlinear drive of 1, yielding (a) $\beta = 0.5$, $\alpha = 24.1^\circ$, (b) $\beta = 1.0$, $\alpha = 24.8^\circ$, (c) $\beta = 1.5$, $\alpha = 28.8^\circ$, and (d) $\beta = 3.0$, $\alpha = 24.2^\circ$.

Fig. 12 shows the nonlinear drive dependence of the maximum conversion efficiency and the rotation angle at which this maximum occurs, for various values of β . The conversion efficiency increases steadily with increasing nonlinear drive, reaches a plateau, and begins to decrease at very high drive

values. We observe that the conversion efficiency is close to its maximum value for a large range of the nonlinear drive, especially above a drive of 1. This saturation value for the conversion efficiency depends on β in a cyclical fashion, its maxima occurring close to β values that are odd integers. For

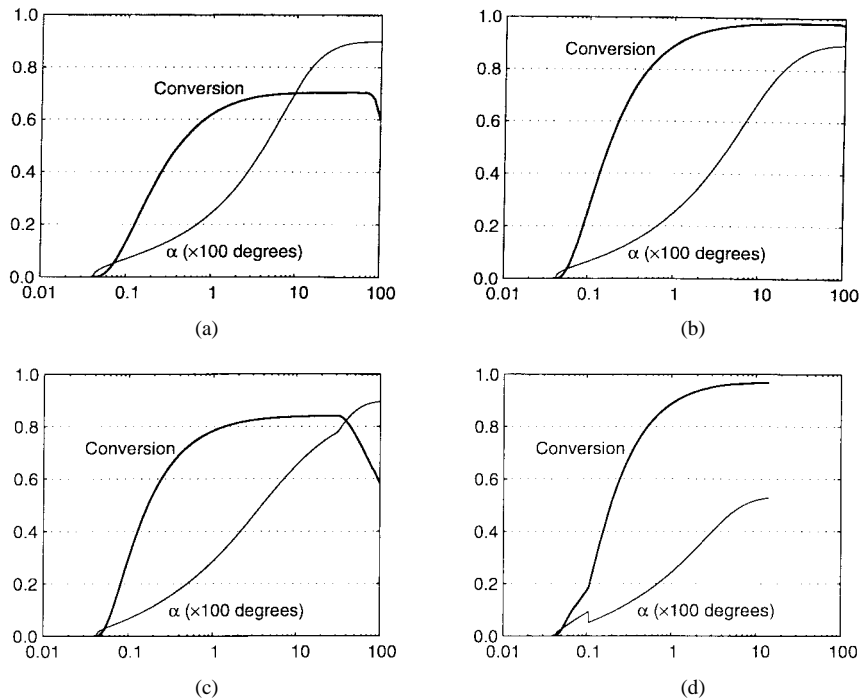


Fig. 12. Maximum conversion efficiency and the polarization rotation angle at which maximum conversion occurs, as functions of the nonlinear drive for class-C self-doubling OPO's for various values of β : (a) $\beta = 0.5$, (b) $\beta = 1.0$, (c) $\beta = 1.5$, and (d) $\beta = 3.0$.

lower values of β , the rotation angle necessary for optimum conversion increases monotonically with increasing nonlinear drive, approaching 90° . For high β values [see Fig. 12(d)], however, abrupt jumps in the optimum α can occur. The reason for this behavior can be seen in the double peaked conversion efficiency curve of Fig. 9; increasing the nonlinear drive has the effect of decreasing the higher peak and increasing the other, and the optimum α makes a sudden jump when the two peaks are equal in magnitude.

V. CONCLUSION

There are six different polarization geometries that can potentially be phase matched for self-doubling OPO's. These polarization geometries can be categorized into three classes depending on the coupled-mode equations that govern each interaction. Class-A self-doubling OPO's can be highly efficient wavelength converters approaching the quantum limit. Furthermore, they are not very sensitive to parameters such as crystal length and pump intensity as long as the SHG interaction is strong. Intracavity polarization rotation is required to achieve frequency-doubling in class-B and class-C self-doubling OPO's. However, class-B OPO's are not expected to be efficient, since the SHG fundamental does not have a resonant component in the cavity. On the other hand, a class-B configuration with 90° polarization rotation results in a situation analogous to intracavity doubling with a second crystal. Class-C self-doubling OPO's can be used for efficient wavelength upconversion, as was experimentally demonstrated by Kartaloğlu *et al.* [9]. Optimum operation can be assured by adjusting the intracavity wave retarder in these OPO's. However, class-C OPO's are more sensitive to variations in

pump intensity. A number of nonlinear crystals that satisfy the simultaneous phase-matching for a variety of pump sources can be identified. Extension of the self-doubling concept to quasi-phase-matched crystals is another promising possibility.

REFERENCES

- [1] *J. Opt. Soc. Amer. B (Special Issue on Optical Parametric Oscillation and Amplification)*, vol. 10, pp. 1659–2243, 1993.
- [2] *J. Opt. Soc. Amer. B (Special Issue on Optical Parametric Devices)*, vol. 12, pp. 2087–2320, 1995.
- [3] C. L. Tang, W. R. Bosenberg, T. Ukachi, R. J. Lane, and L. K. Cheng, "Optical parametric oscillators," *Proc. IEEE*, vol. 80, pp. 365–374, 1992.
- [4] R. J. Ellingson and C. L. Tang, "High-power, high-repetition-rate femtosecond pulses tunable in the visible," *Opt. Lett.*, vol. 18, pp. 438–440, 1993.
- [5] E. C. Cheung, K. Koch, and G. T. Moore, "Frequency upconversion by phase-matched sum-frequency generation in an optical parametric oscillator," *Opt. Lett.*, vol. 19, pp. 1967–1969, 1994.
- [6] P. P. Bey and C. L. Tang, "Plane-wave theory of parametric oscillator and coupled oscillator-upconverter," *IEEE J. Quantum Electron.*, vol. QE-8, pp. 361–369, 1972.
- [7] G. T. Moore, K. Koch, and E. C. Cheung, "Optical parametric oscillation with intracavity second-harmonic generation," *Opt. Commun.*, vol. 113, pp. 463–470, 1995.
- [8] G. T. Moore and K. Koch, "Optical parametric oscillation with intracavity sum-frequency generation," *IEEE J. Quantum Electron.*, vol. 29, pp. 961–969, 1993.
- [9] T. Kartaloğlu, K. G. Köprülü, and O. Aytür, "Phase-matched self-doubling optical parametric oscillator," *Opt. Lett.*, vol. 22, pp. 280–282, 1997.
- [10] R. W. Boyd, *Nonlinear Optics*. San Diego, CA: Academic, 1992.
- [11] R. A. Baumgartner and R. L. Byer, "Optical parametric amplification," *IEEE J. Quantum Electron.*, vol. QE-15, pp. 432–444, 1979.
- [12] J. Yao, W. Sheng, and W. Shi, "Accurate calculation of the optimum phase-matching parameters in three-wave interactions with biaxial nonlinear-optical crystals," *J. Opt. Soc. Amer. B*, vol. 9, pp. 891–902, 1992.
- [13] D. A. Roberts, "Simplified characterization of uniaxial and biaxial nonlinear optical crystals," *IEEE J. Quantum Electron.*, vol. 28, pp. 2057–2074, 1992.



Orhan Aytür (M'94) was born in Ankara, Turkey, in 1965. He received the B.S. degree in electrical engineering from Middle East Technical University, Ankara, Turkey, in 1986, and the M.S. and Ph.D. degrees in electrical engineering from Northwestern University, Evanston, IL, in 1988 and 1991, respectively.

He worked as a Laser Scientist at Fibertek, Inc., in Virginia, and as a Research Associate at the University of New Mexico, Albuquerque, in 1991–1992.

He joined the Department of Electrical Engineering at Bilkent University, Ankara, Turkey, in 1993, where he is presently an Associate Professor. His main research interests include nonlinear frequency conversion of lasers, quantum optics, and high-performance photodetectors.



Yamaç Dikmelik (S'93) was born in Izmir, Turkey, in 1974. He received the B.S. degree in electrical engineering from Bilkent University, Ankara, Turkey, in 1996. He is presently a graduate student at the same institution.

His current research interest is the modeling of synchronously pumped optical parametric oscillators.